Empirical Ocean Colour Algorithms for Estimating Sea Surface Salinity in Coastal Water of Terengganu

Md. Suffian, I.[1]*, Nurhafiza, R.[2] and Noor Hazwani, M. A.[2]

[1]*School of Marine and Environmental Sciences, Universiti Malaysia Terengganu, 21030 Kuala Terengganu, Terengganu, Malaysia*
[2]*Institute of Oceanography and Environment, Universiti Malaysia Terengganu, 21030 Kuala Terengganu, Terengganu, Malaysia*

ABSTRACT

This study presents an empirical approach for estimating sea surface salinity (SSS) from remote sensing of ocean colour. The analysis is based on two important empirical relationships of in-water optical properties. The first involves the behaviour of the optical properties of coloured dissolved organic matter (CDOM) under conservative mixing along the salinity gradient. The second is the tight relationship between CDOM and water-leaving radiance. Our results showed that CDOM absorption coefficients in ultra-violet wavelengths (350 and 380 nm) can be best estimated using the blue-green band ratio $R_{rs}(412/547)$ with a R^2 value of 0.87. It was also found that the absorption coefficient of CDOM in the study area was tightly correlated with the salinity ($R^2 \approx 0.83$); however, the data indicate that this relationship may be dependent on freshwater flow and the intensity of vertical mixing. During the wet and well-mixed season (Northeast monsoon), CDOM was almost conservative with salinity but tended to behave non-conservatively during the dry and stratified season (Southwest monsoon). These resulting empirical relationships allow CDOM and salinity in the study area to be estimated from satellite ocean colour data. Validation using independent datasets showed that the algorithms for CDOM and salinity perform relatively well with the RMS error of 0.04 m^{-1} and 0.30`, respectively, over a range of salinity from 30` to 33`. The ability of the algorithm to predict salinity as those presented in this study can be further improved using more independent tests with *in-situ* and satellite bio-optical measurements.

Keywords: Salinity, ocean colour, empirical algorithms, coloured dissolved organic matter, South China Sea

INTRODUCTION

Sea surface salinity (SSS), one of the main drivers of ocean circulation, plays a vital role in determining the distribution of many

aquatic organisms and influences seawater density and ocean water column stability. Especially in coastal and estuarine environments, the combined effect of temperature and salinity changes can have wide-ranging impacts on the community composition, reproduction, and seasonality processes of aquatic organisms (Barange & Perry, 2009). Even small changes such as future salinity shifts (Boyer et al., 2005) would, therefore, have significant ecological effects on coastal and marine ecosystems, prompting a critical need for a spatially and temporally continuous monitoring of SSS in these environments. Global observations of SSS from space are now available with the recent launches of NASA`s Aquarius and ESA's Soil Moisture and Ocean Salinity (SMOS) missions. Both satellites are capable of retrieving SSS across the world`s oceans and detecting changes as small as 0.2`. Despite these advantages, the coarse spatial and temporal resolution of Aquarius (150 km scale and seven-day revisit) and SMOS (250 km scale and 10-30 day revisit) may prove to be a major limitation for observing SSS in coastal environments. This is in sharp contrast with the daily global 1-km SST and ocean colour properties (chlorophyll, suspended sediment and CDOM) that have been routinely observed using MODIS and other sensors for several decades (Cracknell & Hayes, 2007; McClain, 2009).

Many studies have shown that detritus and CDOM can be good tracers of salinity especially in the coastal ocean (e.g. Del Vecchio & Blough, 2004, Vodacek et al., 1997). CDOM is one of the most important absorbing components in aquatic ecosystems and plays a major role in many physical, chemical and biological processes. Due to strong absorption in the UV and blue portion of the visible spectrum, CDOM can alter the optical properties of natural waters and primary productivity and reduce UV-related damage on marine organisms. In coastal waters with direct sources of terrestrial organic matter, CDOM levels are relatively much higher and more variable than those in the open ocean. In these areas, CDOM thus becomes the major determinant of optical properties and it can behave conservatively during river-ocean mixing. Under the influence of terrestrial sources and conservative mixing, CDOM in coastal waters is often found to be inversely correlated with salinity (Binding & Bowers, 2003; Ahn et al., 2008). Due to the distinct optical signature, CDOM can be easily detected by optical sensors and thus, serves as a relative measure of salinity from ocean colour remote sensing. The tight relationship between blue-green reflectance ratios and the optical properties of CDOM have been reported in many studies (e.g. Mannino et al., 2008; Del Vecchio & Blough, 2004) and this empirical relationship is also found to work well even in a wide range of water types. It is important to note that estimating SSS from remote observations not only requires a clear relationship between CDOM and remote sensing reflectance (R_{rs}), but there must exist a conservative mixing between fresh-high CDOM river waters and salty-low CDOM seawater.

This study aims to estimate SSS from satellite ocean colour remote sensing and is the first to report the possibility of using CDOM as a proxy to salinity in east coast Malaysia water. The objectives necessary to achieve this goal are twofold. Firstly, to investigate the relationships between CDOM and spectral ratios of R_{rs} and between salinity and CDOM using in-situ bio-optical and salinity datasets collected during different monsoon seasons. Secondly, to explore the feasibility and investigate the possibility of using CDOM as a proxy for salinity.

MATERIALS AND METHODS

Data were collected in east coast Malaysia water (Figure 1) during seven bio-optical cruises over the period May to November 2009 and July 2013 onboard a 15-m coastal research boat operated by University Malaysia Terengganu. The study area represented the southern part of the South China Sea (SSCS) and the collection of data coincided with three major monsoon seasons: the Southwest monsoon (June to August), Northeast monsoon (November) and Inter-Monsoon monsoons (May and October). The Northeast monsoon generally brings heavy rain and stronger wind especially on the east coast of Peninsular Malaysia while the Southwest monsoon is a warm period, with generally weaker southwesterly/southerly wind. The inter-monsoonal periods are characterised by unpredictable wind speed and direction. Although it is difficult to determine the actual timing of each monsoon onset, the monsoon intra-seasonal oscillation is a relatively repeatable large scale phenomenon and its timing may vary by two to three weeks (Lau & Yang, 1997; Hoyos & Webster, 2007). The in-situ measurements at 32 stations were performed along inshore-offshore transect that extended up to 60 km offshore, wide enough to compare to satellite imagery. Following a recommendation by Werdell et al. (2003), all measurements were carried out within a time window of 3-4 hours of local noon (no earlier than 0900 or later than 1500 hours) to ensure adequate solar illumination for radiometric measurements. In total, 178 in-situ measurements of underwater radiometric and surface CDOM were performed during the course of this study.

All water samples were collected from approximately 0.5 m depth using 10L dark bottles for absorption measurements. Vertical profiles of hydrological parameters of temperature and salinity were determined using a CTD and YSI (Yellow Springs Instruments, OH, USA) multi-parameter monitoring system. These instruments used the Practical Salinity Scale to measure salinity and did not have units. Measurements of underwater vertical profiles of upwelling radiance, $L_u(z,\lambda)$, and downwelling irradiance, $E_d(z,\lambda)$, were acquired at each location using a Satlantic Hyper OCR from subsurface (0.5 m) to a 10-m depth over 3-m intervals. Hyper OCR data were processed by the Prosoft data analysis package (Satlantic Inc) to Level 2 in which reference and data dark deglitching and correction were applied. Remote sensing reflectance, $R_{rs}(\lambda)$, was then estimated according to:

$$R_{rs}(\lambda) = 0.543\left(\frac{L_u(0^+,\lambda)}{E_d(0^+,\lambda)}\right) \tag{1}$$

where 0.543 is a factor for propagating the radiance through the air-sea interface (Muller et al., 2003).

Following a recommendation by Mueller et al. (2003), a small volume of water (~150 ml) was collected by filtering the samples through 0.2 μm Whatman Nucleopore polycarbonate filters into pre-acid washed and pre-combusted amber glass bottles. The samples were immediately stored cooled in the dark until analysis in order to prevent any potential bleaching effect from the light. Optical densities of CDOM, denoted here as $a_g(\lambda)$, where λ is the wavelength, were measured using a Cary-100 dual beam spectrophotometer in 250 to 800 nm at 1 nm intervals. A separate scan with milli-Q water in both the reference and the sample cells was used as

a reference. The absorption coefficient at 443 nm was selected as a reference wavelength to represent the $a_g(\lambda)$ as calculated from Eq.(2).

$$a_g(\lambda) = 2.303(A_{443} - A_{750})/0.1 \qquad [2]$$

where A_{443} and A_{750} are the absorbances measured at 443 and 750 nm, respectively. The constant of 2.303 is a conversion factor to convert the natural log to base 10 and 0.1 is the cell path length in metres.
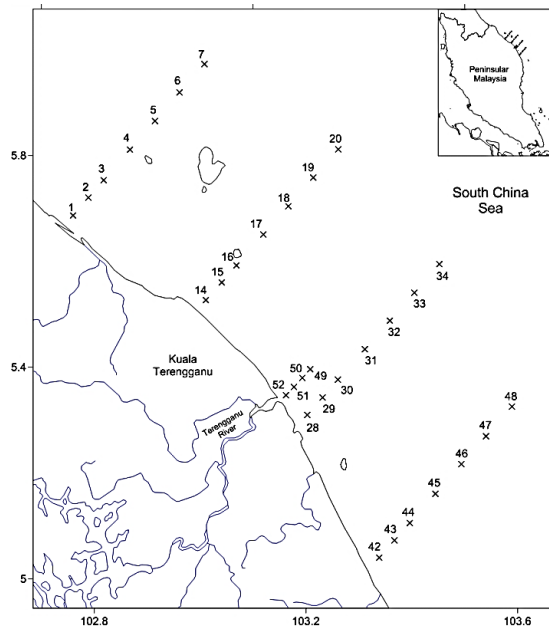
Figure 1. Locations of the sampling stations in the east coast of Peninsular Malaysia water. The sampling stations were visited from May to November 2009 and July 2013

Assessment Statistics

Overall algorithm performances and their uncertainties were assessed by comparing their predicted values (X_{est}) with those measured (X_{mea}) in the field and laboratory. Systematic and random errors of this comparison were quantified based upon two statistical approaches: mean, absolute percentage difference (APD) and root mean square (RMS).

$$\text{APD} = \frac{1}{N}\sum_{n=1}^{N}\left|\left(\frac{X_{est}-X_{mea}}{X_{mea}}\right)\right| * 100 \qquad [3]$$

$$\text{RMS} = [\frac{1}{N}\sum_{n=1}^{N}(X_{est}-X_{mea})^2]^{\frac{1}{2}} * 100 \qquad [4]$$

To indicate the covariance between the X_{mea} and X_{est}, we also quantified the R^2 (regression, type II) coefficient from the correlation analysis.

RESULTS AND DISCUSSION

Seasonal Variability of CDOM and Salinity

Table 1 summarises the data range of $a_g(443)$ and surface salinity measured during the field measurements. Since our sampling stations covered both coastal and offshore waters, a large variation of the $a_g(443)$ and salinity were observed during the cruises, which resulted in the large standard deviation shown in Table 1. Measured individual $a_g(443)$ values clearly showed a decreasing trend from May to October but were sharply increased in November. Relatively clear waters with low $a_g(443)$ values during June to October were found at almost all stations, ranging from 0.02 to 0.18 m^{-1}. During this period, higher values were only observed along the coastal stations especially at stations located very close to the mouth of the Kuala Terengganu river (stations 28, 50 to 52). With initiation of the Northeast monsoon season in November, there was indication of monsoon impact with high wind speed enhancing turbulence in the water column and large river discharge resulting in a dramatic increase of $a_g(443)$. During this season, high $a_g(443)$ was observed not only at coastal regions but stretching out into the offshore water. The $a_g(443)$ during this period varied from 0.01 m^{-1} at the offshore water to 0.43 m^{-1} at the river mouth with an average value of 0.15 m^{-1} (SD=0.12).

In general, the variation of salinity in the study area was influenced by monsoonal wind patterns and the introduction of freshwater especially from the Kuala Terengganu river during the rainy seasons. Seasonally, the surface salinity in the study area ranged from 22` to 33`, with the lowest value observed during the November cruise. As can be seen in Table 1, the largest range of salinity occurred in November, corresponding to large river discharges emptying into the coastal region and the intrusion of high salinity and colder water masses from the South China Sea. During this season, a plume of low salinity water (< 25) was observed to stretch out for 10 km from the Kuala Terengganu river mouth. During the other seasons, low surface salinity was only observed at stations close to the river mouth (stations 51 and 52), that is under direct influence of freshwater discharge.

Table 1
*Mean, Min-Max (Numbers in Bracket) and Standard Deviation (Indicated by a * Sign) of $a_g(443)$ and Surface Salinity During the Sampling Periods*

	May	Jun	Jul	Aug	Oct	Nov
$a_g(443)$ (m^{-1})	0.09	0.06	0.05	0.06	0.04	0.15
	(0.01-0.38)	(0.03-0.18)	(0.02-018)	(0.02-0.11)	(0.02-0.13)	(0.01-0.43)
	0.09*	0.04*	0.04*	0.03	0.03*	0.12*
Salinity	30.9	31.8	32.0	32.3	32.0	29.6
	(24.4-32.2)	(26.1-33.5)	(25.1-33.2)	(28.3-32.9)	(29.4-32.8)	(22.3-32.8)
	1.9*	1.7*	1.5*	0.9*	0.8*	2.9*

Estimation of CDOM from In-Situ Remote Sensing Reflectance (Rrs)

To estimate the $a_g(\lambda)$, we examined empirical relationships between $a_g(\lambda)$ at a specified wavelength in the UV and short blue part of the spectrum (350-443 nm) and three spectral ratios

of R_{rs}(412, 443 and 488)/ (547). A basic assumption underlying the use of these band ratios is that variations in $R_{rs}(\lambda)$ at blue wavelengths are driven largely by changes in the absorption coefficients of seawater, especially due to varying amounts of $a_g(\lambda)$, while variations in the green are mostly affected by particle scattering (Belanger et al., 2008). Regression analysis indicates that all spectral band ratios can be correlated using a power function with $a_g(\lambda)$. Although the correlation was not high, an examination of the statistical relationship of the three band ratios found that the band ratio R_{rs}(412/547) gives the most precise estimates of $a_g(\lambda)$ (for all band ratios, R^2 ranged from 0.87-0.78). Considering all absorption coefficients examined, our results showed that $a_g(\lambda)$ at the UV wavelengths (350 and 380 nm) can be best estimated using this band ratio. As can be seen in Figure 2, absorption at both wavelengths showed close agreement and provided relatively high R^2 (0.87) and small RMS (<7%) values. At least for our dataset, least squares linear regression on $a_g(350)$ and $a_g(380)$ against R_{rs}(412/547) produced the relationship:

$$a_g(350) = 0.2461[R_{rs}(412)/R_{rs}(547)]^{-0.91}$$ [5]

$$a_g(380) = 0.1530[R_{rs}(412)/R_{rs}(547)]^{-0.94}$$ [6]

The strong relationship at these wavelengths suggested that the UV part of the spectrum seemed to be relatively more important for estimating the non-algal products compared with the blue wavelengths. As $a_g(\lambda)$ absorbs more light in the UV region and decreases exponentially with increasing wavelength, a reduced correlation observed for $a_g(\lambda)$ at higher wavelengths (400 to 443 nm) might be expected. Considering the strong influence of $a_g(\lambda)$) on R_{rs}(412), these results are very promising taking into account that only a few band ratio algorithms specially designed to estimate $a_g(\lambda)$ have been published until now (e.g. Mannino et al., 2008; Kowalczuk et al., 2010). In contrast to our finding, most of the published band ratio algorithms for the retrieval of $a_g(\lambda)$ use reflectance values at the chlorophyll peak wavelength of 443 nm or longer. The use of different reflectance values in our band ratio algorithms for $a_g(\lambda)$ retrieval is obviously an advantage as both constituents do not compete for the photons of the same wavelength. This could also improve the sensitivity of empirical algorithms for retrieving $a_g(\lambda)$ and chlorophyll concentrations. In addition, a previous study by Bowers et al. (2012) on the bio-optical characteristics in this area has shown that $a_g(\lambda)$ was the main absorber of light at the short blue wavelengths, so it is expected that other absorption components have little influence on the derived empirical relationships of equations [5] and [6].
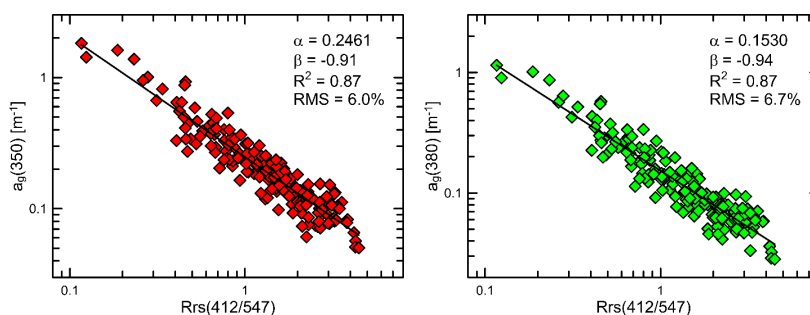
Figure 2. Absorption coefficient of CDOM at 350 and 380 nm as a function of band ratio R_{rs}(412/547). β=regression coefficient/slope, α=intercept, and p<0.05 is significant

Relationship Between Salinity and CDOM Absorption

Figure 3 shows the relationship between $a_g(\lambda)$ at 350 and 380 nm and salinity for all sampled seasons. In general $a_g(\lambda)$ at both wavelengths co-varied linearly and inversely with salinity, suggesting a strong terrestrial origin of $a_g(\lambda)$) in the study area. Within a salinity range from 22` to 33`, a least square regression produced the relationship:

$$Salinity = -5.19[a_g(350)]+32.97 \qquad\qquad [7]$$

$$Salinity = -8.22[a_g(380)]+32.94 \qquad\qquad [8]$$

with $R^2 \approx 0.8$ and RMS ≈ 0.4` for both $a_g(\lambda)$. These findings are consistent with a number of previous studies in other regions (e.g. Binding & Bowers, 2003; Ahn et al., 2008) though there were differences in the regression coefficients (α and β). Linear relationship in Figure 3 reveals, at least for this dataset, that $a_g(\lambda)$ behaved conservatively with respect to salinity and hence could be used to predict salinity. The most conservative $a_g(\lambda)$ mixing was found in November when particularly strong river-ocean mixing (salinity of 22` at Stn 52) was found in the inshore regions. A high coefficient of determination (R^2=0.97) for this data (not shown) is also associated with strong river discharges and a well-mixed water column during those sampling periods. As can be seen in Figure 4, the $a_g(\lambda)$ level clearly responded to the fluctuations in river flow, showing a significant fall and rise over the study period. Weekly Kuala Terengganu river discharge was greatest during November, which may be responsible for the high level of $a_g(\lambda)$ and low surface salinity during this month. This large river flow is fuelled by heavy northeast monsoon rainfall that led to extraordinary sediment transport downstream. On the other hand, the combined effects of strong wind-driven mixing by the monsoonal winds resulted in increased concentration of $a_g(\lambda)$ when deep mixing brought elevated subsurface $a_g(\lambda)$ to the surface layer. During periods of low river discharge and highly stratified mixed layer (May to October), $a_g(\lambda)$ in the study area generally does not behave conservatively (scattered points in Figure 3) with R^2 ranged from 0.1 to 0.4 (not shown). This temporal variability in the relationship between salinity and $a_g(\lambda)$ undoubtedly affected the overall prediction accuracy of our proposed algorithms.
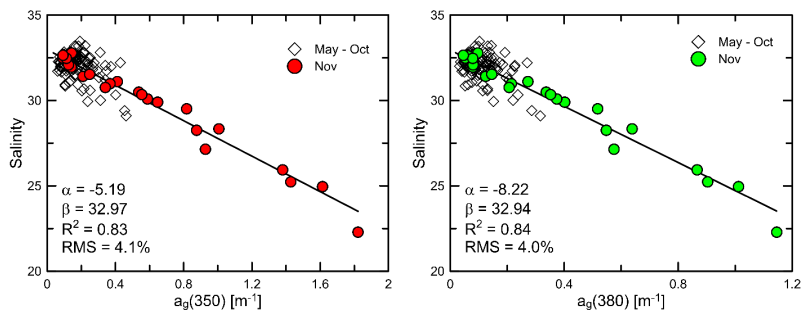
Figure 3. Salinity as a function of absorption coefficient of $a_g(\lambda)$ at 350 and 380 nm. β=regression coefficient/slope, α=intercept and $p<0.05$ is significant
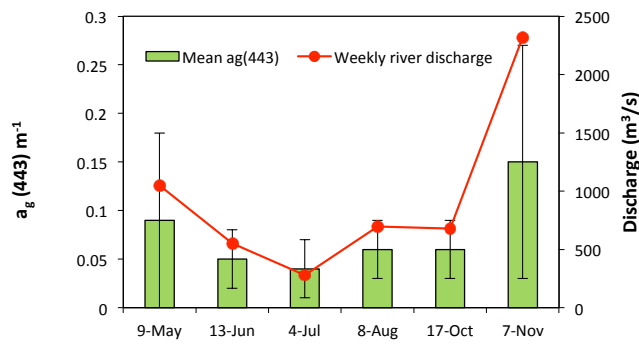
Figure 4. Mean and standard deviation of surface $a_g(443)$, and weekly mean river discharge from the Kuala Terengganu river from May to November 2009 (Data source: Department of Irrigation and Drainage [DID] Malaysia)

Validation of CDOM Absorption and Salinity

Given the significant empirical relationships, it was decided to test the validity of the resultant algorithms by comparing both $a_g(\lambda)$ and salinity values derived from the model and in-situ measurements. We used independent datasets collected during June 2009 and July 2013 to provide a better idea about the performance of both algorithms for estimating $a_g(\lambda)$ and surface salinity. Overall, 29 and 33 in-situ data of surface salinity and $a_g(\lambda)$, respectively, were used for the analysis. It was found that the R_{rs}-derived $a_g(\lambda)$ for both wavelengths (Figure 5, upper panel) fit the in-situ data quite well with a slope of almost unity, RMS error of between 0.03 and 0.04 m^{-1} and the average difference of less than 14% for $a_g(\lambda)$ in the range of 0.01 to 1.5 m^{-1}. These results demonstrate that $a_g(\lambda)$ can be accurately derived from the empirical approach of the remote sensing technique even for this wide range of $a_g(\lambda)$ values. Figure 5 (lower panel) compares the results of surface salinity derived from the model and in-situ measurements for a salinity range from 30` to 33`. Both the algorithms produce quite satisfactory results (RMS≈0.30) and show close agreement between the two measurements (APD≈1.0%). The results suggest that the salinity algorithm is sensitive to fluctuations in $a_g(\lambda)$ levels and has the potential to provide accurate observations of synoptic salinity fields from satellite

remote sensing. While these empirical algorithms work satisfactorily in the study area, more independent validation with in-situ and satellite bio-optical measurements needs to be done to test the performance of the algorithms across a wider range of water types.

Figure 5:
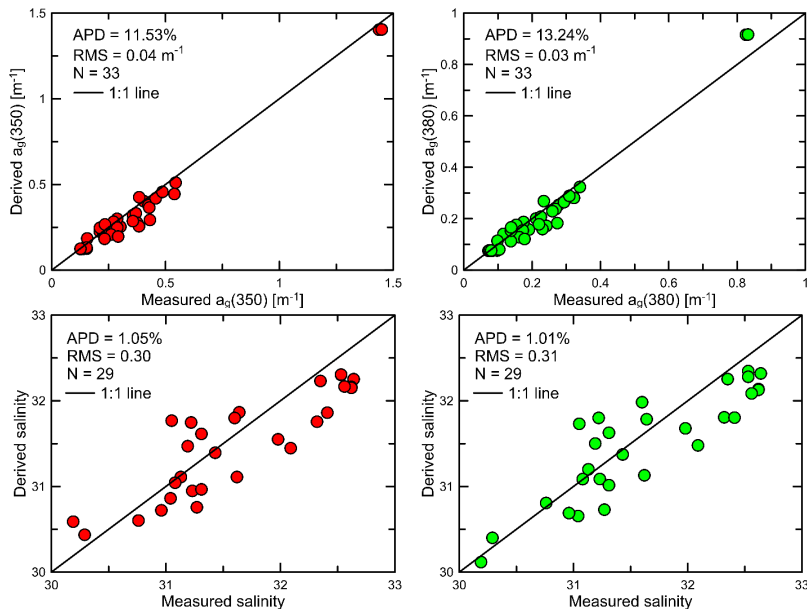
Figure 5. Comparisons of model-derived and field observations of $a_g(\lambda)$ at 350 and 380 nm (upper panel) and salinity (lower panel). The solid line represents the 1:1 line

CONCLUSION

In summary, our study showed that it was indeed possible to estimate SSS on the basis of remote sensing in the region of study. The empirical algorithm using $a_g(\lambda)$ as a proxy presented in this study showed a good estimate of SSS. The ability of algorithms to retrieve SSS through optical remote sensing will ultimately lead to a better understanding of the spatial and temporal variability of physical and biogeochemical processes especially in coastal water. We do note, however, that the algorithm performance may be particularly dependent on the source of $a_g(\lambda)$ and mixing processes, thus, its reliability and applicability may vary by season and region.

ACKNOWLEDGEMENT

REFERENCES

Ahn, Y. H., Shanmugam, P., Moon, J. E., & Ryu, J. H. (2008). Satellite remote sensing of a low-salinity plume in the East China Sea. *Annals of Geophysics, 26*(7), 2019–2035.

Barange, M., & Perry, R. I. (2009). Physical and ecological impacts of climate change relevant to marine and inland capture fisheries and aquaculture. In K. Cochrane, C. De Young, D. Soto, & T. Bahri (Eds.), *Climate change implications for fisheries and aquaculture: Overview of current scientific knowledge* (pp. 7–106). Rome.

Belanger, S., Babin, M., & Larouche, P. (2008). An empirical algorithm for estimating the contribution of chromophoric dissolved organic matter to total light absorption in optically complex waters. *Journal of Geophysical Research, 113*(C4), 1-14, doi: 10.1029/2007JC004436.

Binding, C. E., & Bowers, D. G. (2003). Measuring the salinity of the Clyde Sea from remotely sensed ocean colour. *Estuarine, Coastal and Shelf Science, 57*(4), 605–611.

Bowers, D. G., Md-Suffian, I., & Mitchelson-Jacob, E. G. (2012). Bio-optical properties of east coast Malaysia waters in relation to remote sensing of chlorophyll. *International Journal of Remote Sensing, 33*(1), 150–169.

Boyer, T. P., Levitus, S., Antonov, J. I., Locarnini, R. A., & Garcia, H. E. (2005). Linear trends in salinity for the World Ocean, 1955–1998. *Geophysical Research Letters, 32*(1), 1-4.

Cracknell, A. P., & Hayes, L. (2007). *Introduction to remote sensing.* Boca Raton, Florida: CRC Press.

Del Vecchio, R., & Blough, N. V. (2004). Spatial and seasonal distribution of chromophoric dissolved organic matter and dissolved organic carbon in the Middle Atlantic Bight. *Marine Chemistry, 89*(1), 169–187.

Hoyos, C. D., & Webster, P. J. (2007). The role of intraseasonal variability in the nature of Asian monsoon precipitation. *Journal of Climate, 20*(17), 4402–4424.

Kowalczuk, P., Cooper, W. J., Durako, M. J., Kahn, A. E., Gonsior, M., & Young, H. (2010). Characterization of dissolved organic matter fluorescence in the South Atlantic Bight with use of PARAFAC model: Relationships between fluorescence and its components, absorption coefficients and organic carbon concentrations. *Marine Chemistry, 118*(1), 22–36.

Lau, K. M., & Yang, S. (1997). Climatology and interannual variability of the Southeast Asian Summer Monsoon. *Advances in Atmospheric Sciences, 14*(2), 141–162.

Mannino, A., Russ, M. E., & Hooker, S. B. (2008). Algorithm development and validation for satellite-derived distributions of DOC and CDOM in the US Middle Atlantic Bight. *Journal of Geophysical. Research-Oceans, 113*(C7), 1-19. doi:10.1029/2007JC004493.

McClain, C. R. (2009). A decade of satellite ocean color observations. *Annual Review of Marine Science, 1*, 19–42.

Mueller, J. L., Fargion, G. S., McClain, C. R., Pegau, S., Zanefeld, J. R. V., Mitchell, B. G., ... & Stramska, M. (2003). *Ocean optics protocols for Satellite Ocean color sensor validation* (Revision 4, Volume I-VI.). National Aeronautics and Space Administration.

Vodacek, A., Blough, N. V., De Grandpre, M. D., Peltzer, E. T., & Nelson, R. K. (1997). Seasonal variation of CDOM and DOC in the Middle Atlantic Bight: Terrestrial inputs and photo oxidation. *Limnology and Oceanography, 42*(4), 674–686.

Werdell, P. J., Bailey, S., Fargion, G., Pietras, C., Knobelspiesse, K., Feldman, G., & McClain, C. (2003). Unique data repository facilitates ocean color satellite validation. *Eos, Transactions American Geophysical Union, 84*(38), 377–392.